Research Article | Vol. 27, No. 8 | 15 Apr 2019 | OPTICS EXPRESS A445
Optics EXPRESS

Optimal satellite orbit configuration for global ocean color product coverage

KARLIS MIKELSONS[1,2,*] AND MENGHUA WANG[1]

[1]NOAA/NESDIS Center for Satellite Applications and Research, 5830 University Research Ct., College Park, Maryland 20740, USA
[2]Global Science and Technology, Inc., Greenbelt, Maryland 20770, USA
*karlis.mikelsons@noaa.gov

Abstract: We develop a methodology to evaluate the current orbital configuration of the Visible Infrared Imaging Radiometer Suite (VIIRS) onboard the Suomi National Polar-orbiting Partnership (SNPP) and NOAA-20 satellites and to study various orbital configurations for the next VIIRS in the Joint Polar Satellite System (JPSS) series from the perspective of maximizing the global daily ocean color retrievals. We focus on the coverage losses due to high sensor-zenith angle and high sun glint contamination and find that two sensors cannot avoid gaps in daily coverage. If JPSS-2 shares the same orbit with SNPP and NOAA-20, then phase shift of around 90° relative to SNPP and NOAA-20 would maximize daily ocean color retrievals.

1. Introduction

We are now living in the era of rapidly expanding Earth observations from space, but also at the time when rapid changes in Earth environment are taking place. Ocean optical, biological, and biogeochemical products are essential for understanding of climate change and its impact on our daily life, and satellite ocean color observations are indispensable means to accurate and timely global picture, as well as routine global water quality monitoring and quantitative measurements [1–3].

The Joint Polar Satellite System (JPSS) program [4] aims to deliver consistent global daily records of Earth observations spanning multiple decades using a series of satellites carrying sensors of similar design and capabilities. The Suomi National Polar-orbiting Partnership (SNPP) satellite, which was launched on October 28, 2011, is the precursor to the JPSS satellite series. SNPP is flying in polar sun synchronous daytime ascending orbit with inclination of 98.7° and local equatorial crossing time around 13:30 for the location under nadir. The Visible Infrared Imaging Radiometer Suite (VIIRS) is one of the instruments flying aboard SNPP satellite and has been (and will be) carried on the subsequent JPSS satellites. VIIRS is a whiskbroom scanner type imager and has 22 spectral bands in the range 0.41–12 μm [5], which are used for a wide range of Earth land, atmosphere, and ocean (including coastal/inland waters) observations [4]. In particular, VIIRS-derived global ocean color Environmental Data Records (EDR) is one of the key product suites for science research and application communities [6,7].

SNPP is followed by NOAA-20, which was launched on November 18, 2017, and is the first operational satellite in the JPSS series. NOAA-20 carries the same instrument package as SNPP, including VIIRS, and is also flying in practically the same daytime ascending polar orbit. However, the position on the orbit (phase) of NOAA-20 is shifted by 180° (time difference of about 50 minutes on the orbit) relative to SNPP. Beyond NOAA-20, the next satellite in JPSS series (carrying the same VIIRS) is scheduled to be launched around 2021.

While the designed lifetime of JPSS satellites is about 7 years, in the past similar satellite missions, e.g., the Moderate Resolution Imaging Spectroradiometer (MODIS) [8] on the Terra (1999–present) and Aqua (2002–present), have significantly exceeded their designed

#358998 https://doi.org/10.1364/OE.27.00A445
Journal © 2019 Received 29 Jan 2019; revised 1 Mar 2019; accepted 4 Mar 2019; published 20 Mar 2019

Optics EXPRESS

lifetime, and continued to provide useful observations for many years beyond it. The possibility of overlapping satellite missions by multiple sensors of the same design raises the question of how to arrange their orbits to maximize the utility of the observations. This question is especially relevant to the global ocean color retrievals, since the rate of valid global daily ocean color data retrievals is rather small (e.g., as low as ~5% for some retrieval algorithms [9]), due to clouds [10], straylight [11], sun glint [12], and other factors. Merging data from different sensors can improve the overall data coverage [13], but the improvement depends on the configuration of the sensor orbits. Thus, in this paper, we investigate the question of optimal configuration for polar orbiting satellites from the perspective of the global ocean color observations.

The remainder of the paper is structured as follows: we first discuss the main factors limiting satellite ocean color retrievals in Section 2, and show how they affect the single sensor ocean color data coverage in Section 3. We then show in Section 4 how multiple satellite sensors in different positions on the same orbit can be modeled using data from a single sensor. We will then proceed to apply this method to investigate various orbit configurations of two and three sensors in Sections 5 and 6, and evaluate the effects on the ocean color data coverage. Section 7 provides discussion and summarizes the findings.

2. VIIRS ocean color measurements

Deriving global ocean optical, biological, and biogeochemical properties from space-based measurements requires accounting for various light scattering processes in the atmosphere and at the water surface, through a procedure known as atmospheric correction [14–16]. It converts the top of the atmosphere (TOA) radiance spectra measured from space into the normalized water-leaving radiance spectra $nL_w(\lambda)$ [17–19], from which various optical, biological, and biogeochemical property data, e.g., chlorophyll-a (Chl-a) concentration [20–22], water diffuse attenuation coefficient at the wavelength of 490 nm $K_d(490)$ [23,24] or at the domain of the photosynthetically available radiation (PAR) $K_d(\text{PAR})$ [25,26], are further derived. The NOAA VIIRS ocean color retrievals use the Multi-Sensor Level-1 to Level-2 (MSL12) ocean color data processing system [6], which was developed for consistent ocean color data processing from various satellite ocean color sensors [27]. MSL12 has been significantly updated to improve VIIRS global ocean color products, in particular, over turbid coastal and inland waters [28–31]. In addition, VIIRS on-orbit vicarious calibration has been carried out using the in situ optics data from the Marine Optical Buoy (MOBY) in waters off Hawaii [32,33].

In satellite ocean color remote sensing, one of the most significant limiting factors for valid ocean color data retrievals is the cloud cover [10], i.e., ocean color data retrievals are only possible over clear sky [34]. While areas with small and fast-moving clouds may be observed with multiple sensors at different times of day [35], possibly yielding more complete merged coverage from multiple sensors, large cyclone systems can prevent ocean color data retrievals over vast areas for several days.

Another, closely related, major limiting factor affecting ocean color data product retrievals is the cloud-adjacent straylight effect, often resulting in low-quality data near clouds [11,36]. Traditional methods flag these likely low-quality ocean color data according to instrument point spread functions [37], so they are not used in global ocean color data composites. However, a recent study based on spectral analysis showed that such a flagging is perhaps too conservative [11]. Nevertheless, cloud-adjacent straylight vastly expands the data gaps, especially in the areas with sparse clouds [11].

In the polar areas, where the sun is below horizon for many days every year, ocean color retrievals are also not possible for extended periods of time. In fact, good quality ocean color retrievals are only possible when solar-zenith angle is less than ~70°. For larger value of solar-zenith angle, the ocean color retrievals are affected by scattering of the incident sunlight through a long path of atmosphere [15,16], compounded by Earth's curvature effects [38],

and thus deemed as not reliable. Thus, near spring and fall equinoxes, satellite ocean color retrievals are restricted to latitudes less than 70°. During the winter solstice, however, the Earth's axial tilt of 23.4° further restricts the ocean color retrievals to the latitudes less than 70° – 23.4° = 46.6° (while enabling more retrievals around the opposite polar area). Since this factor affects all space-based ocean color retrievals nearly equally, we are not considering it in this study.

VIIRS features a wide swath which extends up to 56.28° off the nadir view, and measures at around 3040 km on ground [39], allowing for some overlap of swaths from the adjacent orbits, even on the equator. The swath edges correspond to the sensor-zenith angle of around 70°. However, the data quality of the ocean color retrievals for large sensor-zenith angles near swath edge is very significantly reduced [14–16,40]. For that reason, the effective swath width for good quality ocean color retrievals is restricted to sensor-zenith angles less than 60°, leading to gaps between adjacent orbits in ocean color coverage in tropics (see Fig. 1 in the next section). In MSL12, ocean color data are processed for all possible solar- and sensor-zenith angles. However, for high solar- or sensor-zenith angles, global ocean color data are masked out in the Level-3 ocean color products. The upper limits for the solar- and sensor-zenith angles for the data masking are set as constant.

Reflection of sun light from ocean surface (sun glint) [41] is another significant limiting factor for ocean color retrievals [12]. The sun glint mostly affects the retrievals in the tropical areas, but it has a seasonal modulation, and can reach the latitudes as high as 50° for days near summer solstice [35]. For a sensor on the polar orbit with local afternoon equatorial overpass, the solar reflection off the ocean surface is mostly west from the nadir view. The actual extent of the sun glint areas is determined not just by the solar and sensor geometry, but also by the water surface roughness, which is strongly correlated to the ocean surface wind speed [42]. In addition, for atmospheric correction in MSL12, the TOA radiance computation (e.g., Rayleigh scattering radiance) requires accurate surface sun glint information [42,43]. Thus, there is no simple and exact criterion to identify the areas with high sun glint. The current NOAA VIIRS ocean color retrievals in MSL12 use the value of glint coefficient [12] of 0.01 computed from the Cox and Munk model [41] as a threshold value beyond which the retrievals are considered as high sun glint contaminated, and may have large errors in satellite-derived ocean color products [12].

While clouds, low sunlight, straylight, large sensor-zenith angle, and high sun glint are major limiting factors for ocean color retrievals, the latter two – high sensor-zenith angle and high sun glint contamination – directly depend on the choice of the sensor orbit, and can be mitigated by combining data from two or more satellite sensors [13]. In this study, we investigate what orbital configurations of two and three sensors minimize the data gaps by these two factors that affect global daily ocean color data product coverage.

3. Single sensor global ocean color coverage

Different factors limiting ocean color retrievals from a single satellite sensor can be identified in daily VIIRS-SNPP Chl-a imagery, after discarding low-quality data (i.e., those associated with the various quality control flags), shown in Fig. 1 for September 21, 2018. This day is close to the fall equinox, so that both northern and southern hemispheres are equally well illuminated. The true color base layer in Fig. 1(a) provides a complete daily global coverage, including land. The overlaid Chl-a imagery, however, cannot be derived over land, in areas with clouds, ice, dense dust, etc. Areas with high sensor-zenith angles and high sun glint contamination are also excluded. Note that Chl-a data presented and discussed in this study are derived using the OCI Chl-a algorithm implemented in MSL12 [22].

Figure 1(b) highlights the gaps in data due to high sensor-zenith angles and high sun glint contamination – the focus of this study. The data gaps due to high sensor-zenith angle always occur in tropics near the swath edges and result in relatively narrow gaps spanning latitudes of 35°S–35°N, which do not change with season. The areas with high sun glint contamination

are the wider gaps spanning smaller range in latitudes, shifting with seasonal modulation. These areas can also be identified by the characteristic sun glint pattern in the true color imagery [Fig. 1(a)]. Since SNPP is in daytime ascending orbit, its daytime orbital track follows southeast to northwest direction. The data gaps due to high sensor-zenith angle and high sun glint contamination are also aligned with the orbital track. We note that in Fig. 1(b) we have combined ocean color data from three days separated by the SNPP revisit interval of 16 days to emphasize these areas, minimizing the other data gaps due to clouds. The purpose of using the three-day composite images is to clearly demonstrate (visually) the effects of data gaps due to high sensor-zenith angle and high sun glint contamination on the coverage of satellite ocean color retrievals.

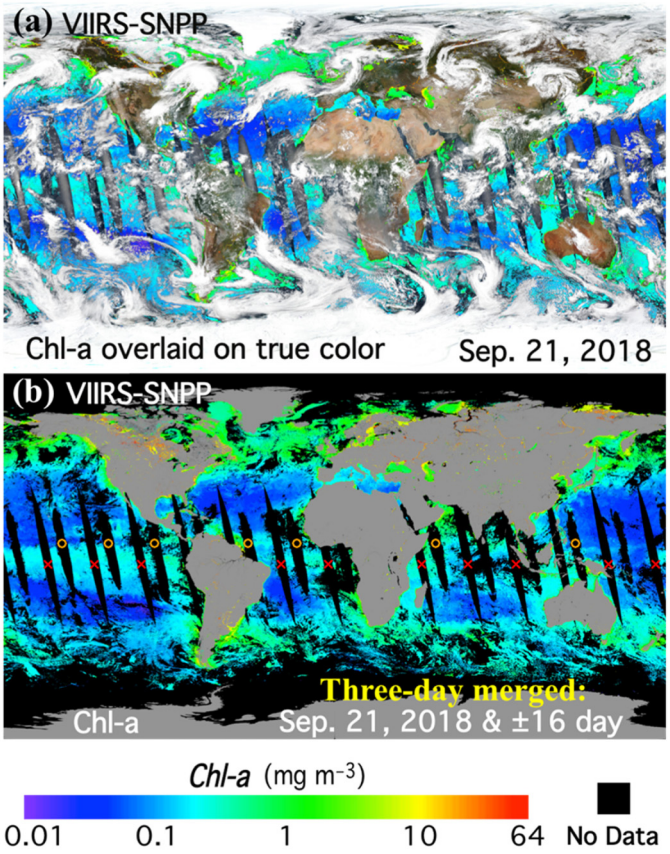

Fig. 1. (a) VIIRS-SNPP Chl-a data overlaid on top of true color imagery, showing daily coverage for September 21, 2018. Even though true color has a complete global coverage, ocean color products cannot be derived (or are masked) in areas with clouds, high sun glint, high sensor-zenith angle, and polar areas with little sunlight (i.e., large solar-zenith angle). (b) Combined VIIRS-SNPP Chl-a data coverage for three days separated by SNPP 16-day revisit cycle, showing fewer gaps due to clouds and emphasizing gaps due to high sensor-zenith angles (some marked with red crosses) and high sun glint (some marked with orange circles).

To quantify the extent of these data gaps, or the loss of ocean color data coverage due to high sensor-zenith angle and high sun glint contamination, we have used the VIIRS-SNPP ocean color data (binned at 9 km resolution) from the entire year 2016, and calculated for each day the area where ocean color retrievals were not possible due to either of the two conditions. We also calculate for each day the total global area that has receives enough sunlight (i.e., solar-zenith angle less than 70°) during one of VIIRS-SNPP overpasses, as well as the total area of valid ocean color retrievals. These results are displayed in Fig. 2. In fact,

Optics EXPRESS

the total area of open waters that receives enough sunlight for ocean color retrievals changes with the season, with maxima around spring and fall equinoxes. The absolute minimum occurs near northern hemisphere summer solstice when significant parts of the Southern Ocean are under dark. The area lost from single sensor ocean color retrievals due to high sensor-zenith angle does not change throughout the year and amounts to ~9.3%, while the area subject to high sun glint has a slight seasonal variation, averaging ~9.4% throughout the year. Of the remaining ~81.3%, clouds and other factors involving atmospheric conditions prohibit retrievals for ~66% of remaining area, resulting in ocean color retrievals for only ~28% of the total area of open and sunlit waters over the course of the year. We note again that these numbers are based on statistics for 9 km bins. Thus, if even one valid retrieval falls within a given bin, the whole bin is counted towards the area with valid ocean color retrievals.

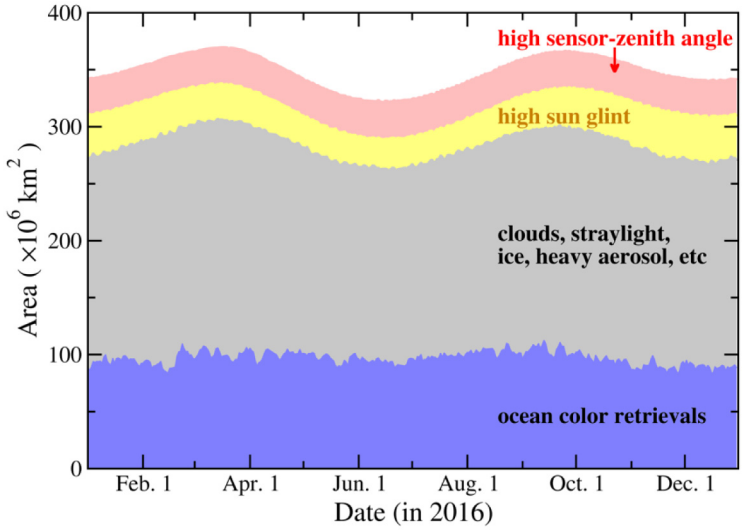

Fig. 2. Seasonal dependence of the total water surface area illuminated by sunlight, including the area of valid ocean color retrievals (blue), the areas where clouds, straylight, ice, dust and heavy aerosols prevent ocean color retrievals (gray), the area high sun glint (yellow), and of high sensor-zenith angle (pink).

4. Modelling multiple sensors orbital configurations

Both SNPP and NOAA-20 are flying in the same orbit with a 16-day revisit cycle, completing 227 full orbits during this time period. Thus, on each day, both satellites complete 14 full orbits, and a fraction (3/16) of 15th orbit. During one orbit, the Earth rotates by 25.374° about its axis, and 14 orbits correspond to Earth rotating by 355.24°. Thus, on the following day, all the orbital tracks are shifted by 360° – 355.24° = 4.76° east. This introduces a phase shift of 3/16 × 360° = 67.5° on the next day orbits, relative to the given day. In fact, this is also equal to the fraction of the 15th orbit completed at the end of each day. Since NOAA-20 is shifted in orbit by 180° relative to SNPP, on any given day NOAA-20 orbits have the same ground tracks as SNPP orbits eight days before or after the given day. The dependence of the phase shift with respect to time difference in days is illustrated in Fig. 3.

We can therefore use the VIIRS-SNPP ocean color data from different consecutive days to model another sensor on the same orbit, but with a different phase relative to SNPP. In the following sections, we will explore the combinations of two and three sensors flying on the same orbit with different relative phase shifts, and assess the effects on the coverage of the merged ocean color data products.

Optics EXPRESS

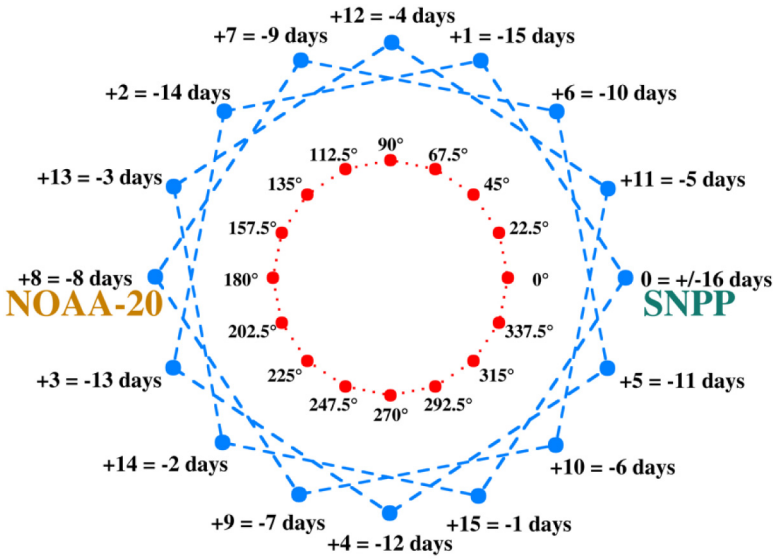

Fig. 3. SNPP 16-day revisit cycle with phase shifts corresponding to time shift in days relative to the SNPP orbit on the given day. Each day introduces a phase shift of 67.5°, resulting in zero phase shift after 16 days. NOAA-20 is flying in the same orbit as SNPP, but 180° out of phase, which also corresponds to SNPP orbit from ± 8 days relative to the present day.

5. Two-sensor global ocean color coverage

In this section, we study the combination of two sensors on the same orbit as SNPP but with a variable phase shift, to determine what configuration maximizes ocean color retrievals. This evaluates the current SNPP and NOAA-20 configuration based on the combined ocean color product coverage, and also accounts for a scenario where SNPP is replaced with JPSS-2 on the same orbit, with the latter continuing observations together with NOAA-20.

To model the combined ocean color data coverage by two sensors, we merge VIIRS-SNPP data from different days with time difference corresponding to the phase shift according to Fig. 3. Thus, for example, to model a sensor with a phase shift $\varphi = 22.5°$ ahead of SNPP in the same orbit, we can use the SNPP data from either 5 days before or 11 days after the selected day. However, for two identical sensors, the merged coverage only depends on the absolute value of the relative phase between them, thus we can equally well choose to use the SNPP data from 5 days after or 11 days before the selected day to model the same phase shift. Therefore, in addition to the VIIRS-SNPP data on a particular day of interest, we choose the data from the closest following day that yields the desired phase shift between the two sensors. The corresponding time differences in days are shown in Table 1.

Since all the patterns in data gaps occur with the same interval because of SNPP revisit cycle of 16 days, for better visualization we again supplement the data for each of the two days with additional data from 16 days before and 16 days after the given day. This significantly increases the combined coverage and highlights the remaining data gaps (due to high sensor-zenith angle and high sun glint contamination). In general, the areas with high sun glint shift with a seasonal modulation, but this effect is relatively small over the 32-day period. Thus, to produce representative imagery, each choice of phase shift is modeled by merging VIIRS-SNPP data from six days (i.e., three days for each of the two sensors).

Optics EXPRESS

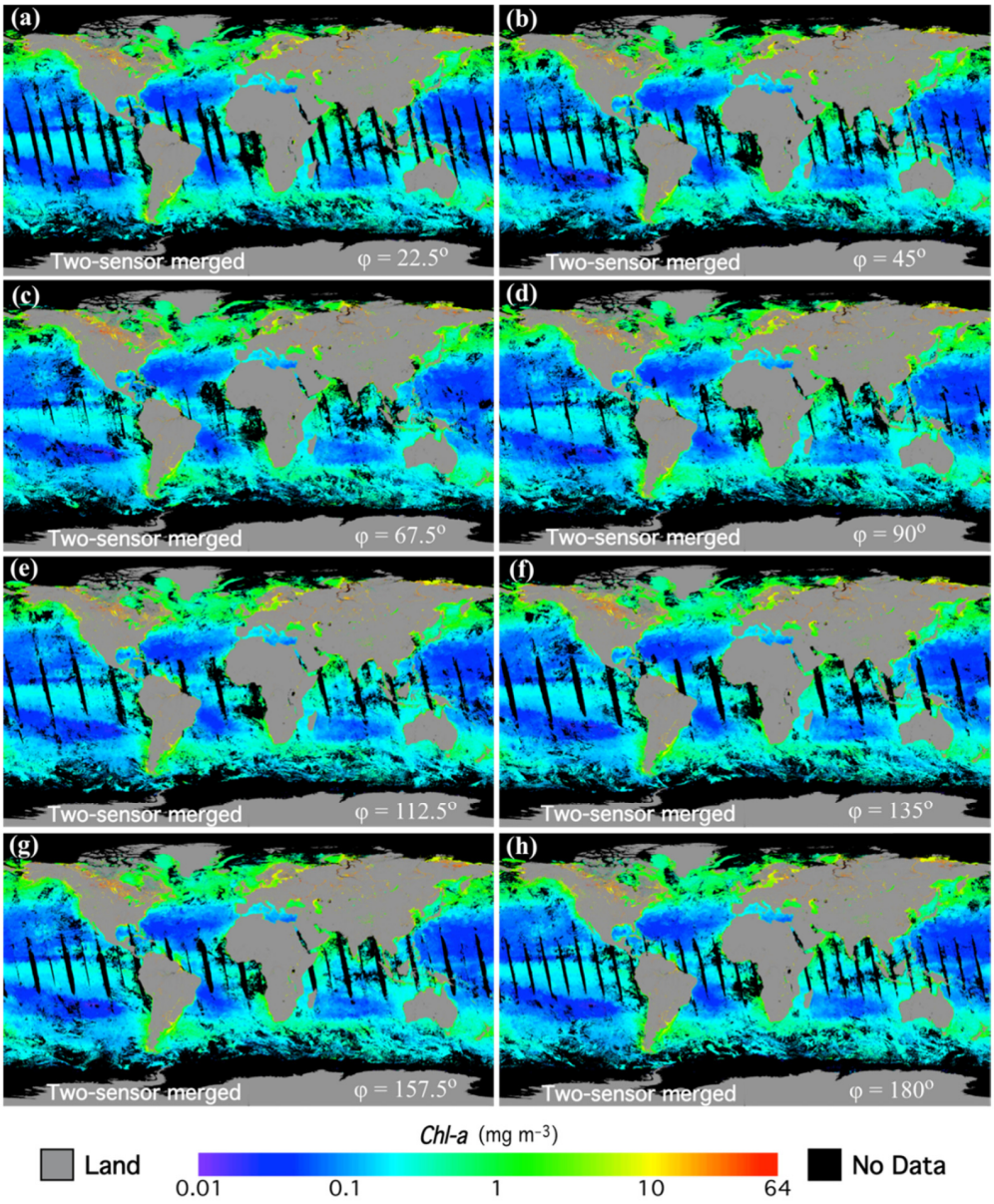

Fig. 4. Merged coverage of global Chl-a imagery on September 21, 2018 from VIIRS-SNPP with data from different days used to model two sensors on the same orbit with a variable relative phase shift φ of (a) 22.5°, (b) 45°, (c) 67.5°, (d) 90°, (e) 112.5°, (f) 135°, (g) 157.5°, and (h) 180°. Note that for more complete coverage and to highlight the remaining data gaps due to high sensor-zenith angle and high sun glint conditions, data for each day is supplemented with data from 16 days before and after, which have the same pattern of data gaps.

Specifically, Figs. 4(a)–4(h) were generated using VIIRS-SNPP-derived global Chl-a data on September 21, 2018 combined with the VIIRS-SNPP Chl-a data derived in 2018 on September 26 [Fig. 4(a)], September 27 [Fig. 4(b)], September 22 [Fig. 4(c)], September 25 [Fig. 4(d)], September 28 [Fig. 4(e)], September 23 [Fig. 4(f)], September 24 [Fig. 4(g)], and September 29 [Fig. 4(h)], respectively. As discussed previously, VIIRS-SNPP global Chl-a data on the specific day are supplemented (merged) by the VIIRS-SNPP data acquired on ±

16 days on that specific day to reduce the data gaps due to clouds and to emphasize gaps because of high sensor-zenith angle and high sun glint contamination.

As seen in Fig. 4, the ocean color data (Chl-a) coverage losses due to high sensor-zenith angle and high sun glint contamination are minimized when the phase shift between the two sensors in the same orbit is from 67.5°–90°, even though for this range there are still some gaps remaining. As mentioned, for two sensors, the coverage loss for phase shift of $-\varphi$ is the same as for φ. The present phase shift of 180° between SNPP and NOAA-20 results in a little more data gaps. This is easily understood if we recall that the regions of high sun glint are relatively close to the center of the VIIRS-SNPP scan (see Fig. 1). Thus, a phase shift of 180° overlays the swath edge (with high sensor-zenith angle) for one sensor and the swath center (with high sun glint) for the another, leading to a gap in the combined/merged coverage.

As for a single sensor, we quantify the coverage loss using the VIIRS-SNPP ocean color data for the entire year 2016. For merged data from two sensors, this coverage loss depends on their relative phase in the orbit (φ), or more precisely, on the absolute value $|\varphi|$ of the phase shift (coverage is an even function of φ), and thus we only need to investigate values of φ in the range from 0°–180°. We show this dependence for the aggregated ratio for the entire year of data in Table 1. Table 1 also provides the time difference (in minutes) on orbit corresponding to the phase shift, e.g., 180° phase shift between the two sensors (SNPP and NOAA-20) is about 50 minutes in the orbit difference. The dependence of the coverage loss on the relative phase shift angle φ is consistent with changes in imagery with angle φ in Fig. 4, with minimum coverage loss for the values of phase shift angle φ between 67.5° and 90°. However, it should be noted that even with the 180° phase shift between the two sensors, as in the case for SNPP and NOAA-20, the global ocean color data gap is significantly reduced (from 18.7% to 6.4%).

Table 1. Loss of the ocean color product coverage due to high sensor-zenith angle (> 60°) and high sun glint conditions. VIIRS-SNPP ocean color data from year 2016 are used to simulate the merged data from two sensors on the same orbit as SNPP, but with a relative phase shift of φ. Phase shift of 67.5°–90° minimizes the coverage losses, but no choice of phase shift allows to completely eliminate data gaps due to these factors.

Phase shift φ	Time difference on orbit (minutes)	Time difference of merged data (days)	Coverage loss (%)
0°	0	0	18.7
22.5°	6.3	5	11.9
45°	12.7	6	6.48
67.5°	19.0	1	2.88
90°	25.4	4	2.72
112.5°	31.7	7	4.28
135°	38.1	2	5.70
157.5°	44.4	3	6.25
180°	50.8	8	6.36

6. Three-sensor global ocean color coverage

With three sensors, the general analysis for optimal orbit configuration becomes more complicated as there are two independent variables (i.e., two phase shifts) describing the configuration. However, since SNPP and NOAA-20 have been flying with a 180° phase shift, we focus on the scenario where these two sensors continue in the current configuration, and the third sensor (JPSS-2) is added in the same orbit with a variable phase shift φ. The results of the three-sensor merged Chl-a data imagery for various phase shifts are shown in Fig. 5.

Optics EXPRESS

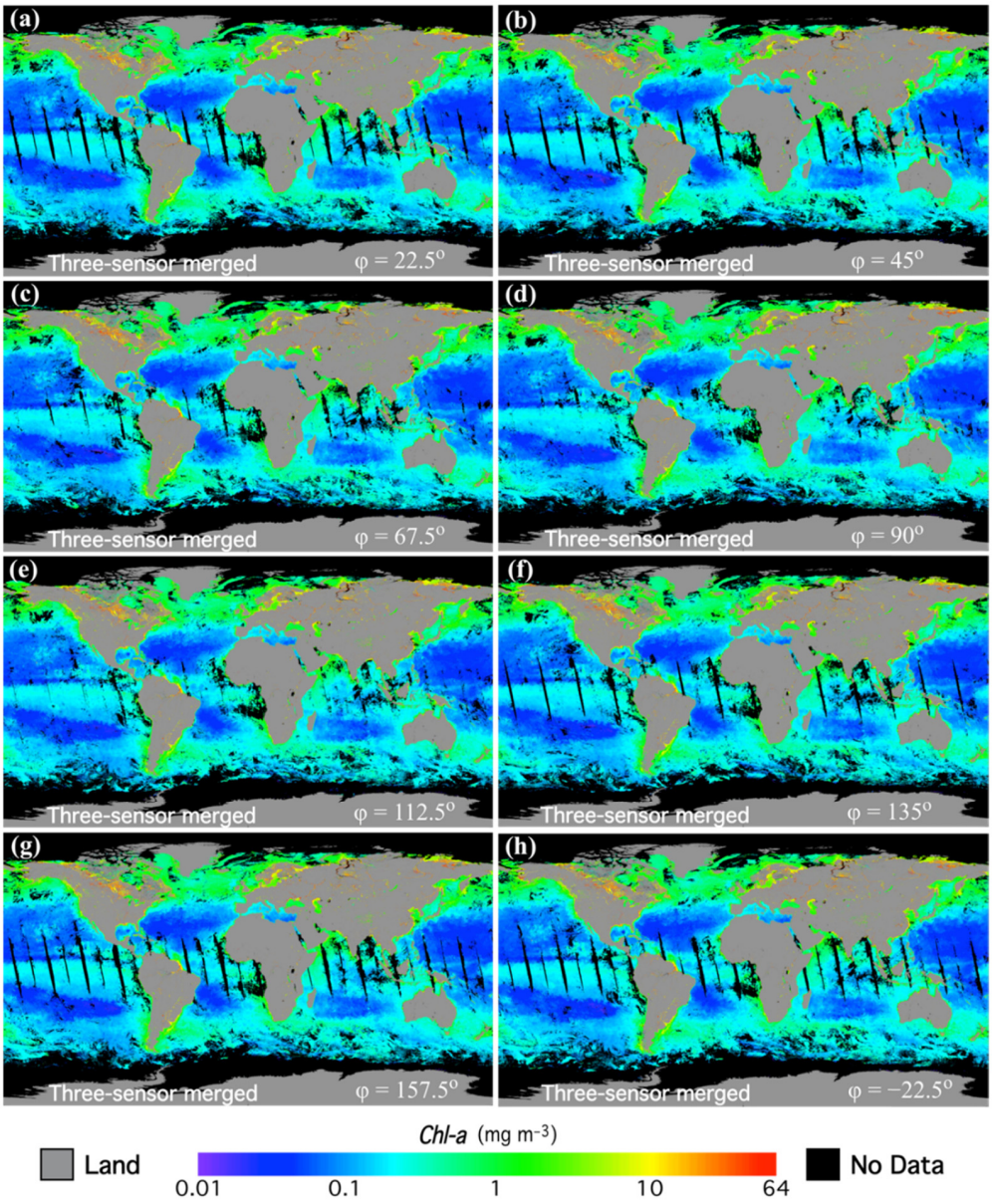

Fig. 5. Three-sensor merged global daily Chl-a imagery on September 21, 2018 with the two sensors from SNPP and NOAA-20, and third one simulated assuming the relative phase shift φ to SNPP of (a) 22.5°, (b) 45°, (c) 67.5°, (d) 90°, (e) 112.5°, (f) 135°, (g) 157.5°, and (h) –22.5°. As before, data for each day is supplemented by the data from 16 days before and after, to minimize the gaps due to clouds and to highlight the gaps due to high sensor-zenith angle and high sun glint contamination. Note that due to symmetry, the extent and pattern of data gaps in panels (g) φ = 157.5° and (h) φ = 157.5° – 180° = –22.5° is essentially identical.

Here, we use the merged ocean color data from VIIRS SNPP and NOAA-20 to model these two sensors, and VIIRS-SNPP data shifted in time to model the third sensor with a phase shift φ with respect to SNPP. We use the fact that SNPP and NOAA-20 are exactly opposite in the orbit (phase shift of 180°), to show that due to symmetry, the coverage of the resultant three-sensor combined data product will be the same for phase shifts φ and φ + 180°. Thus, again, only the values of φ within 0°–180° need to be considered. For example, to

model the three-sensor coverage with the third sensor flying 22.5° ahead of SNPP, we use the merged SNPP and NOAA-20 data from the day of interest, and the SNPP data from five days before. The time differences in days required to model different phase shifts are shown in Table 2.

As in the case of two sensors, we use the data from 16 days before and after to minimize the gaps due to clouds, and to highlight the gaps due to high sensor-zenith angle and high sun glint contamination. Thus, each choice of phase shift in the three-sensor combined imagery is modeled by merging SNPP data from six days and NOAA-20 data from three days.

As shown in Fig. 5, with three sensors, the gaps in data are minimized when the third sensor is placed on the same orbit with a phase shift φ of 90°–112.5° ahead of SNPP or NOAA-20 (i.e., with orbit time difference of 25–32 minutes). The slight departure of the optimal phase shift from 90° is due to high sun glint conditions occurring mostly on the west side from the scan center. Other choices of φ closer to either 0° or 180° (meaning closer on the orbit to SNPP or NOAA-20) result in progressively increasing gaps in the combined (three-sensor) coverage. As mentioned, the coverage is the same for phase shifts φ and φ + 180°. This is illustrated in Fig. 5 panels (g) φ = 157.5° and (h) φ = 157.5° – 180° = –22.5°, which show essentially identical pattern of data gaps.

As for two sensors, we also show the quantitative loss of the coverage due to high sensor-zenith angle and high sun glint contamination for a three-sensor combined data product in Table 2. The quantitative values are obtained using VIIRS-SNPP data for the entire year 2016, and the dependence on the phase shift angle (or time difference in orbit) for the third sensor is consistent with imagery in Fig. 5. The coverage loss is less than one percent for the phase shift φ in the range of 90°–112.5° (or orbit time difference of 25–32 minutes).

Table 2. Loss of the three-sensor mixed ocean color product coverage due to high sensor-zenith angle (> 60°) and high sun glint conditions. VIIRS-SNPP ocean color data from year 2016 are used to simulate the merged data from the three sensors on the same orbit as SNPP, but with different phases (φ), i.e., SNPP: φ = 0°; NOAA-20: φ = 180°; and the third sensor (JPSS-2) with variable φ. Phase shift of 90°–112.5° for the third sensor relative to SNPP or NOAA-20 minimizes and practically eliminates the coverage losses due to high sensor-zenith angle and high sun glint contamination.

Phase shift φ	Time difference on orbit (minutes)	Time difference of merged data (days)	Coverage loss (%)
0°	0	0	6.36
22.5°	6.3	–5	4.05
45°	12.7	+6	2.78
67.5°	19.0	+1	1.76
90°	25.4	–4	0.73
112.5°	31.7	+7	0.53
135°	38.1	+2	1.88
157.5°	44.4	–3	3.93
180°	50.8	±8	6.36
–22.5°	–6.3	+5	3.93

In the unlikely case of four sensors sharing the same orbit, the most obvious choice is to have them separated by equal 90° phase shifts. Because this choice of phase shift maximizes the ocean color product coverage in two- or three-sensor configuration, it would only increase the coverage with four sensors, eliminating data gaps due to high sensor-zenith angle or high sun glint contamination. However, the fourth sensor may have to replace the first one due to sensor aging and accuracy degradation, which likely becomes significant after the sensor designed life time is exceeded.

7. Discussion and summary

Besides the cloud cover, straylight, and insufficient sunlight, the two main factors limiting polar orbiting satellite ocean color retrievals are the high sensor-zenith angle for retrievals

Optics EXPRESS

near the swath edges, and the high sun glint conditions in tropics near the center of the swath. In this paper, we have studied the impact of these two factors on the combined daily ocean color data coverage from two or three sensors, by using the data from VIIRS-SNPP and VIIRS-NOAA-20 to model various orbital configurations of identical sensors sharing the same orbit.

The current orbital configuration of SNPP and NOAA-20 flying on the same orbit with 180° out of phase (or about 50 minutes in orbit time difference) is not optimal for maximal coverage of ocean color retrievals. This is because the sun glint affected ocean color retrievals are relatively close to the center of swath, which corresponds to the swath edge with high sensor-zenith angle for the other sensor. In fact, a relative phase shift of 67.5° to 90° between the two satellites in orbit would minimize the coverage losses due to these two factors in the two-sensor combined ocean color product coverage. Still, even with the present SNPP and NOAA-20 orbital configuration, the daily global ocean color data gap due to these two factors has been significantly reduced from 18.7% (one sensor) to 6.4% (two sensors). Yet this number could be decreased to 2.7% if the two sensors were to fly separated by a 90° phase shift.

It should be noted that the present orbital configuration for SNPP and NOAA-20, i.e., flying 180° out of phase, may be preferable for other data products, e.g., from land and atmosphere. In addition, a phase shift of 180° maximizes time between observations from the two sensors, increasing the chance that clouds may have shifted, and thus increasing the overall chance of retrievals in areas with sparse clouds. For example, on September 21, 2018, both VIIRS-SNPP and VIIRS-NOAA-20 each produced valid retrievals of ~30.1% over global water surface area that was sufficiently illuminated by the sun (estimated based on a fraction of 9 km bins with valid retrievals). The coverage from the two-sensor merged data for the same day was significantly higher at ~41.5%. More than half (~54%) of this increase in the coverage was due to changes in atmospheric conditions (such as clouds shifting), allowing more retrievals in the areas where neither of the sensors experiences high sun glint, nor high sensor-zenith angle conditions. The rest of the improvement in the coverage was due to filling the data gaps associated with these two conditions.

Further separating the observation times by choosing polar orbits with different equator crossing times (such as in the morning and in the afternoon) may fill even more data gaps due to clouds and straylight [9]. However, a morning orbit is not a likely choice for JPSS-2 satellite, given its role as SNPP (or possibly NOAA-20) replacement, and also the fact that Sentinel-3 series satellites are already flying in a morning orbit.

The remaining data gaps may be filled through machine learning [44], or through other approaches based on spatial-temporal characteristics of the data products, such as the Data Interpolating Empirical Orthogonal Functions (DINEOF) [45–47]. In particular, a recent study shows that using the DINEOF method the gap-filled data based on the merged VIIRS-SNPP and VIIRS-NOAA-20 ocean color data can provide more details in the dynamic ocean features than those from the SNPP or NOAA-20 alone [47]. Still, even with these methods, the gaps in data due to sparse clouds may be easier to fill than the contiguous gaps due to high sensor-zenith angle or high sun glint contamination.

Assuming SNPP and NOAA-20 continue fly in the present configuration with 180° phase shift, and the JPSS-2 joins these two sensors on the same orbit, the daily combined coverage of ocean color retrievals will be maximized if the third sensor is shifted in orbit by a phase of 90° to 112.5° (or orbit time difference of 25–32 minutes), relative to either SNPP or NOAA-20. This would practically eliminate the data gaps in combined ocean color coverage due to coincidental high sensor-zenith angle and high sun glint contamination for different sensors.

JPSS series satellites carry several instruments that are used for a wide variety of Earth observations and have different requirements for the solar-sensor geometry. While this study outlines the ocean color perspective, other Earth observations may have different

requirements. The choice of JPSS-2 orbital parameters will remain a compromise that maximizes benefits for all observations.

Finally, the methodology and approach developed in this study can be used for other satellite observing systems, as well as for other types of Earth observations.

Funding

Joint Polar Satellite System (JPSS); NOAA Product Development, Readiness, and Application (PDRA)/Ocean Remote Sensing (ORS) Program.

Acknowledgements

We thank two anonymous reviewers for their useful comments. The views, opinions, and findings contained in this paper are those of the authors and should not be construed as an official NOAA or U.S. Government position, policy, or decision.

References

1. IOCCG, *Why Ocean Colour? The Societal Benefits of Ocean-Colour Technology*, T. Platt, N. Hoepffner, V. Stuart, and C. Brown (Eds.), Reports of International Ocean-Color Coordinating Group, No. 7, IOCCG, Dartmouth, Canada (2008).
2. C. R. McClain, "A decade of satellite ocean color observations," Annu. Rev. Mar. Sci. **1**(1), 19–42 (2009).
3. IOCCG, *Earth Observations in Support of Global Water Quality Monitoring*, S. Greb, A. Dekker, and C. Binding (Eds.), Reports of International Ocean-Color Coordinating Group, No. 17, IOCCG, Dartmouth, Canada (2018).
4. M. D. Goldberg, H. Kilcoyne, H. Cikanek, and A. Mehta, "Joint Polar Satellite System: The United States next generation civilian polar-orbiting environmental satellite system," J. Geophys. Res. Atmos. **118**(24), 13463–13475 (2013).
5. C. F. Schueler, J. E. Clement, P. E. Ardanuy, C. Welsch, F. DeLuccia, and H. Swenson, ""NPOESS VIIRS sensor design overview," (Proc. SPIE 4483, 2002), doi:10.1117/12.453451.
6. M. Wang, X. Liu, L. Tan, L. Jiang, S. Son, W. Shi, K. Rausch, and K. Voss, "Impact of VIIRS SDR performance on ocean color products," J. Geophys. Res. Atmos. **118**(18), 10347–10360 (2013).
7. M. Wang, L. Jiang, X. Liu, S. Son, J. Sun, W. Shi, L. Tan, K. Mikelsons, X. Wang, and V. Lance, "VIIRS ocean color products: A progress update," in 2016 IEEE International Geoscience and Remote Sensing Symposium (IEEE, 2016), pp. 5848–5851.
8. V. V. Salomonson, W. L. Barnes, P. W. Maymon, H. E. Montgomery, and H. Ostrow, "MODIS: advanced facility instrument for studies of the Earth as a system," IEEE Trans. Geosci. Remote Sens. **27**(2), 145–153 (1989).
9. L. Feng and C. Hu, "Comparison of valid ocean observations between MODIS Terra and Aqua over the global oceans," IEEE Trans. Geosci. Remote Sens. **54**(3), 1575–1585 (2016).
10. M. D. King, S. Platnick, W. P. Menzel, S. A. Ackerman, and P. A. Hubanks, "Spatial and temporal distribution of clouds observed by MODIS onboard the Terra and Aqua satellites," IEEE Trans. Geosci. Remote Sens. **51**(7), 3826–3852 (2013).
11. L. Jiang and M. Wang, "Identification of pixels with stray light and cloud shadow contaminations in the satellite ocean color data processing," Appl. Opt. **52**(27), 6757–6770 (2013).
12. M. Wang and S. W. Bailey, "Correction of the sun glint contamination on the SeaWiFS ocean and atmosphere products," Appl. Opt. **40**(27), 4790–4798 (2001).
13. S. Maritorena, O. H. F. d'Andon, A. Mangin, and D. A. Siegel, "Merged satellite ocean color data products using a bio-optical model: characterisstics, benefits and issues," Remote Sens. Environ. **114**(8), 1791–1804 (2010).
14. H. R. Gordon and M. Wang, "Retrieval of water-leaving radiance and aerosol optical thickness over the oceans with SeaWiFS: a preliminary algorithm," Appl. Opt. **33**(3), 443–452 (1994).
15. M. Wang, "Remote sensing of the ocean contributions from ultraviolet to near-infrared using the shortwave infrared bands: simulations," Appl. Opt. **46**(9), 1535–1547 (2007).
16. IOCCG, *Atmospheric Correction for Remotely-Sensed Ocean-Colour Products*, M. Wang (Ed.), Reports of International Ocean-Color Coordinating Group, No. 10, IOCCG, Dartmouth, Canada (2010).
17. A. Morel and B. Gentili, "Diffuse reflectance of oceanic waters. III. Implication of bidirectionality for the remote-sensing problem," Appl. Opt. **35**(24), 4850–4862 (1996).
18. H. R. Gordon, "Normalized water-leaving radiance: revisiting the influence of surface roughness," Appl. Opt. **44**(2), 241–248 (2005).
19. M. Wang, "Effects of ocean surface reflectance variation with solar elevation on normalized water-leaving radiance," Appl. Opt. **45**(17), 4122–4128 (2006).
20. J. E. O'Reilly, S. Maritorena, B. G. Mitchell, D. A. Siegel, K. L. Carder, S. A. Garver, M. Kahru, and C. R. McClain, "Ocean color chlorophyll algorithms for SeaWiFS," J. Geophys. Res. **103**(C11), 24937–24953 (1998).

Optics EXPRESS

21. C. Hu, Z. Lee, and B. A. Franz, "Chlorophyll a algorithms for oligotrophic oceans: A novel approach based on three-band reflectance difference," J. Geophys. Res. **117**, C01011 (2012).
22. M. Wang and S. Son, "VIIRS-derived chlorophyll-a using the ocean color index method," Remote Sens. Environ. **182**, 141–149 (2016).
23. Z. P. Lee, M. Darecki, K. Carder, C. Davis, D. Stramski, and W. Rhea, "Diffuse attenuation coefficient of downwelling irradiance: An evaluation of remote sensing methods," J. Geophys. Res. **110**(C2), C02017 (2005), doi:10.1029/2004JC002573.
24. M. Wang, S. Son, and J. L. W. Harding, Jr., "Retrieval of diffuse attenuation coefficient in the Chesapeake Bay and turbid ocean regions for satellite ocean color applications," J. Geophys. Res. **114**(C10), C10011 (2009), doi:10.1029/2009JC005286.
25. A. Morel, Y. Huot, B. Gentili, P. J. Werdell, S. B. Hooker, and B. A. Franz, "Examining the consistency of products derived from various ocean color sensors in open ocean (Case 1) waters in the perspective of a multi-sensor approach," Remote Sens. Environ. **111**(1), 69–88 (2007).
26. S. Son and M. Wang, "Diffuse attenuation coefficient of the photosynthetically available radiation Kd(PAR) for global open ocean and coastal waters," Remote Sens. Environ. **159**, 250–258 (2015).
27. M. Wang, A. Isaacman, B. A. Franz, and C. R. McClain, "Ocean-color optical property data derived from the Japanese Ocean Color and Temperature Scanner and the French Polarization and Directionality of the Earth's Reflectances: a comparison study," Appl. Opt. **41**(6), 974–990 (2002).
28. M. Wang and W. Shi, "The NIR-SWIR combined atmospheric correction approach for MODIS ocean color data processing," Opt. Express **15**(24), 15722–15733 (2007).
29. M. Wang, W. Shi, and L. Jiang, "Atmospheric correction using near-infrared bands for satellite ocean color data processing in the turbid western Pacific region," Opt. Express **20**(2), 741–753 (2012).
30. L. Jiang and M. Wang, "Improved near-infrared ocean reflectance correction algorithm for satellite ocean color data processing," Opt. Express **22**(18), 21657–21678 (2014).
31. M. Wang and L. Jiang, "Atmospheric correction using the information from the short blue band," IEEE Trans. Geosci. Remote Sens. **56**(10), 6224–6237 (2018).
32. D. K. Clark, H. R. Gordon, K. J. Voss, Y. Ge, W. Broenkow, and C. Trees, "Validation of atmospheric correction over the ocean," J. Geophys. Res. **102**(D14), 17209–17217 (1997).
33. M. Wang, W. Shi, L. Jiang, and K. Voss, "NIR- and SWIR-based on-orbit vicarious calibrations for satellite ocean color sensors," Opt. Express **24**(18), 20437–20453 (2016).
34. M. Wang and W. Shi, "Cloud masking for ocean color data processing in the coastal regions," IEEE Trans. Geosci. Remote Sens. **44**(11), 3196–3205 (2006).
35. L. Feng, C. Hu, B. B. Barnes, A. Mannino, A. K. Heidinger, K. Strabala, and L. T. Iraci, "Cloud and sun-glint statistics derived from GOES and MODIS observation sover the Intra-Americas Sea for GEO-CAPE mission planning," J. Geophys. Res. Atmos. **122**(3), 1725–1745 (2017).
36. L. Feng and C. Hu, "Cloud adjacency effects on top-of-atmosphere radiance and ocean color data products: A statistical assessment," Remote Sens. Environ. **174**, 301–313 (2016).
37. G. Meister and C. R. McClain, "Point-spread function of the ocean color bands of the Moderate Resolution Imaging Spectroradiometer on Aqua," Appl. Opt. **49**(32), 6276–6285 (2010).
38. K. Ding and H. R. Gordon, "Atmospheric correction of ocean-color sensors: effects of the Earth's curvature," Appl. Opt. **33**(30), 7096–7106 (1994).
39. C. Cao, X. Xiong, R. Wolfe, F. DeLuccia, Q. Liu, S. Blonski, G. Lin, M. Nishihama, D. Pogorzala, H. Oudrari, and D. Hillger, "Visible Infrared Imaging Radiometer Suite (VIIRS) Sensor Data Record (SDR) User's Guide," (NOAA Technical Report NESDIS 142, version 1.3, 2017).
40. B. B. Barnes and C. Hu, "Dependence of satellite ocean color data products on viewing angles: A comparison between SeaWiFS, MODIS, and VIIRS," Remote Sens. Environ. **175**, 120–129 (2016).
41. C. Cox and W. Munk, "Measurements of the roughness of the sea surface from photographs of the sun's glitter," J. Opt. Soc. Am. **44**(11), 838–850 (1954).
42. H. R. Gordon and M. Wang, "Surface-roughness considerations for atmospheric correction of ocean color sensors. I: The Rayleigh-scattering component," Appl. Opt. **31**(21), 4247–4260 (1992).
43. M. Wang, "The Rayleigh lookup tables for the SeaWiFS data processing: Accounting for the effects of ocean surface roughness," Int. J. Remote Sens. **23**(13), 2693–2702 (2002).
44. S. Chen, C. Hu, B. B. Barnes, Y. Xie, G. Lin, and Z. Qiu, "Improving ocean color data coverage through machining learning," Remote Sens. Environ. **222**, 286–302 (2019).
45. J. Beckers and M. Rixen, "EOF calculations and data filling from incomplete oceanographic data sets," J. Atmos. Ocean. Technol. **20**(12), 1839–1856 (2003).
46. A. Alvera-Azcarate, A. Barth, M. Rixen, and J. Beckers, "Reconstruction of incomplete oceanographic data sets using Empirical Orthogonal Functions. Application to the Adriatic Sea," Ocean Model. **9**(4), 325–346 (2005).
47. X. Liu and M. Wang, "Filling the gaps of missing data in the merged VIIRS SNPP/NOAA-20 ocean color product using the DINEOF method," Remote Sens. **11**(2), 178 (2019), doi:10.3390/rs11020178.